



# Performance of supercapacitors with RuO<sub>2</sub> electrodes spray deposited with aqueous/organic solvent mixtures: effect of substrate temperature

R. Chandrashekhar & Abhijit A. Yadav

To cite this article: R. Chandrashekhar & Abhijit A. Yadav (2023): Performance of supercapacitors with RuO<sub>2</sub> electrodes spray deposited with aqueous/organic solvent mixtures: effect of substrate temperature, Phase Transitions, DOI: [10.1080/01411594.2022.2164495](https://doi.org/10.1080/01411594.2022.2164495)

To link to this article: <https://doi.org/10.1080/01411594.2022.2164495>



Published online: 11 Jan 2023.



Submit your article to this journal [↗](#)



View related articles [↗](#)



View Crossmark data [↗](#)



# Performance of supercapacitors with RuO<sub>2</sub> electrodes spray deposited with aqueous/organic solvent mixtures: effect of substrate temperature

R. Chandrashekhar and Abhijit A. Yadav 

Thin Film Physics Laboratory, Department of Physics, Electronics and Photonics, Rajarshi Shahu Mahavidyalaya (Autonomous), Latur, Maharashtra, India

## ABSTRACT

RuO<sub>2</sub> electrodes were spray-deposited utilizing an aqueous/organic solvent mixture at varied substrate temperatures. X-ray diffraction data supported the rutile structure and tetragonal phase of RuO<sub>2</sub>. FESEM images showed a porous structure with small spherical grains covering the entire substrate surface. Optical studies have shown that RuO<sub>2</sub> films have bandgaps between 1.90 and 2.13 eV. Electrical resistivity was found in the range of  $0.57 \times 10^4 \Omega\text{-cm}$  to  $1.23 \times 10^4 \Omega\text{-cm}$ . CV (scan rate  $5 \text{ mVs}^{-1}$ ) results confirmed the specific capacitances of 560, 637, 687, 602 and  $527 \text{ Fg}^{-1}$  at substrate temperatures of 250, 275, 290, 300 and  $325^\circ\text{C}$ , respectively, in  $0.5 \text{ M H}_2\text{SO}_4$  electrolyte. RuO<sub>2</sub> provided a high specific capacitance  $741 \text{ Fg}^{-1}$  (current density  $0.5 \text{ Ag}^{-1}$ ) from GCD profile besides good specific capacitance holding of 87.66% over 3000 continuous charge–discharge cycles. The results show that RuO<sub>2</sub> films spray deposited with aqueous/organic solvent mixtures give the best results.

## ARTICLE HISTORY

Received 17 October 2022  
Accepted 28 December 2022

## KEYWORDS

Spray pyrolysis; RuO<sub>2</sub> thin film; aqueous/organic solvent mixture; supercapacitor; cyclic voltammetry

## 1. Introduction

Energy is crucial for the advancement of humanity [1]. The world economy and environment will suffer greatly if energy production and consumption are dependent on the burning of fossil fuels [2]. The increasing global demand for electrical devices makes it imperative to develop renewable, environmentally friendly, efficient and reliable energy storage devices [3]. Numerous applications that call for the generation or storage of electrical energy need the use of electrical energy storage. A storage device must satisfy all specifications for that application, including those for energy density, power density, weight, size, cost, longevity, etc. [4].

A renewable energy portfolio must include electrochemical energy. The energy storage devices like supercapacitors and batteries/fuel cells work on the electrochemical energy conversion principle. Several groups are working on supercapacitors due to their characteristics including high specific power, extensive cycle life, environmental friendliness, etc. [5–7]. Overall, electric-double-layer capacitors (EDLC) and pseudocapacitors are two types for supercapacitors. An electrical charge is created in a pseudocapacitor by electron transfer that causes a change in the chemical/oxidation state of electrode material depending on Faraday's law. EDLC is non-faradaic; i.e. ideally, there is no electron transfer [8–11].

Currently, most commercial supercapacitor electrodes are fabricated with cheap and corrosion resistive carbon. As the electrodes do not change chemically throughout the charge/discharge

operation, supercapacitors based on carbon provide good cycle stability. However, the active electrode surface area and the distribution of pore sizes limit their maximum capacity (typically  $0.15\text{--}0.4\text{ Fm}^{-2}$  or  $\sim 150\text{ Fg}^{-1}$  for carbon) [12]. Carbon-based EDLC supercapacitors show specific energy  $3\text{--}5\text{ Whkg}^{-1}$ , smaller than  $10\text{--}250\text{ Whkg}^{-1}$  (Li-ion batteries) and  $30\text{--}40\text{ Whkg}^{-1}$  (Pb-acid batteries) [13–15]. For many applications, such a small energy density is insufficient. Therefore, metal oxides are being researched as a working electrode for supercapacitors in order to increase the energy density and specific capacitance [16–19].

The commonly researched metal oxides comprise  $\text{CuO}$ ,  $\text{SnO}_2$ ,  $\text{Co}_3\text{O}_4$ ,  $\text{V}_2\text{O}_5$ ,  $\text{WO}_3$ ,  $\text{MnO}_2$ ,  $\text{Mn}_3\text{O}_4$ ,  $\text{NiO}$ ,  $\text{TiO}_2$ ,  $\text{Fe}_2\text{O}_3$ ,  $\text{NiFe}_2\text{O}_4$ ,  $\text{CoFe}_2\text{O}_4$ ,  $\text{RuO}_2$ , etc. [16–23]. Kour et al. [19] have provided overview of  $\text{MnO}_2$ /Transition metal oxides,  $\text{MnO}_2$ /Transition metal hydroxides, and  $\text{MnO}_2$ /Layered double hydroxides composites for supercapacitor applications. Zhao et al. [17] fabricated  $\text{Co}_3\text{O}_4$ / $\text{NiFe}_2\text{O}_4$  hybrids via a template-free hydro-thermal route. The specific capacitance of  $243.3\text{ Fg}^{-1}$  at  $1\text{ Ag}^{-1}$  has been observed. Fang et al. [18] studied the  $\text{MnO}_2$  electrode on Ni foam in a  $\text{Na}_2\text{SO}_4$ / $\text{KOH}$  mixed electrolyte for supercapacitor applications and obtained a specific capacitance of  $1801\text{ Fg}^{-1}$  at  $5\text{ mVs}^{-1}$ . Earlier we have reported spray-deposited Ni doped  $\text{Mn}_3\text{O}_4$  electrodes with specific capacitance of  $705\text{ Fg}^{-1}$  at  $10\text{ mVs}^{-1}$  [21], spray-deposited NiO electrodes with specific capacitance of  $564\text{ Fg}^{-1}$  at  $5\text{ mVs}^{-1}$  [22] and spray-deposited  $\text{Co}_3\text{O}_4$  nanostructures with specific capacitance of  $425\text{ Fg}^{-1}$  at  $5\text{ mVs}^{-1}$  [23].

According to the literature review, the specific capacitance of metal oxide electrodes is a size order greater than that of carbon electrodes. Numerous studies have demonstrated that bare metal oxide electrodes are capable of producing high power densities and large specific capacitances even at low scan rates. Because of its superior metallic conductivity, wide operating potential window, large specific capacitance, greatly reversible oxidation–reduction reaction, and long-lasting cycle life,  $\text{RuO}_2$  has been extensively researched as a possible contender among these [24,25].

$\text{RuO}_2$  films being deposited utilizing a variety of deposition methods such as thermal evaporation [24], hydro-thermal [26], sputtering [27], electrodeposition [28], solvothermal [29], sol-gel thermal decomposition [30] and spray pyrolysis [31–33]. Among them, spray pyrolysis has a variety of benefits, such as affordability, adaptability, the capacity to produce porous nanostructured films, and suitability for large-scale deposition. In this study,  $\text{RuO}_2$  film electrodes were spray-deposited utilizing an aqueous/organic solvent mixture at varied substrate temperatures. The dependence of  $\text{RuO}_2$  thin film properties on substrate temperature has been investigated.

## 2. Experimental

$\text{RuO}_2$  film electrodes were spray-deposited utilizing an aqueous/organic solvent mixture at varied substrate temperatures  $250$ ,  $275$ ,  $290$ ,  $300$  and  $325^\circ\text{C}$  on glass and conducting glass substrates. The required quantity of ruthenium (III) chloride trihydrate ( $\text{RuCl}_3\cdot 3\text{H}_2\text{O}$ ) was dissolved in freshly made double-distilled water to create a  $25\text{ mM}$  precursor solution. For each deposition,  $10\text{ ml}$  of ruthenium (III) chloride trihydrate solution was taken and mixed with  $10\text{ ml}$  of ethanol. Preparative parameters including precursor solution concentration ( $25\text{ mM}$ ), spray rate ( $3\text{--}4\text{ ml min}^{-1}$ ), nozzle to substrate distance ( $28\text{ cm}$ ), and carrier gas pressure (air;  $176,520\text{ Nm}^{-2}$ ) were optimized using electrochemical technique.

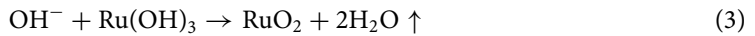
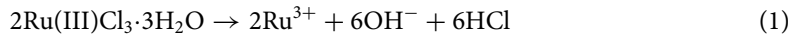
With the use of a  $\text{Cu-K}\alpha$  radiation from X-ray diffractometer (Ultima IV) at a wavelength of  $1.5406\text{ \AA}$ , structural characteristics of  $\text{RuO}_2$  films were explored. Gas porosimetry was used to calculate the pore volume and pore area. The BET surface area was calculated from the porosimetry. A FESEM (S-4800) and EDAX were used for morphological and compositional analysis. To determine optical bandgap, absorption spectra of  $\text{RuO}_2$  films were documented with a UV-Visible spectrophotometer (Ocean Optics JAZ-3 and NIR-QUEST). Electrical conductivity measurements were performed using the DC two-point probe technique.  $\text{RuO}_2$  films were measured electrochemically (CV, GCD and EIS) using an electrochemical analyzer (CHI 608D). A typical three-electrode cell arrangement was adopted, with a  $1\text{ cm}^2$   $\text{RuO}_2$  film functioning as the working electrode and

saturated Ag/AgCl & platinum serving as the reference and counter electrodes in a 0.5 M H<sub>2</sub>SO<sub>4</sub> electrolyte. CV analysis was carried out in a potential range from 0.0 to 1.0 V at different scan rates. GCD experiment was conducted at various current densities (0.5–4 Ag<sup>-1</sup>) within a potential range between 0.0 and 0.85 V. The measurement of electrochemical impedance was performed at 5 mV AC amplitude in the frequency range of 100 kHz–1 Hz.

### 3. Results and discussion

#### 3.1. Growth mechanism

Methanol and ethanol are commonly utilized in the spray deposition of metal oxides. There are no reports that aqueous/organic solvent mixtures were utilized to deposit RuO<sub>2</sub> films. The resultant film has distinct growth kinetics because the reaction and decomposition processes of the spray solution on the substrate are varied for each of the solvents utilized [32,34]. A ruthenium (III) chloride trihydrate (RuCl<sub>3</sub>·3H<sub>2</sub>O) in an aqueous/organic solvent mixture sprayed onto hot substrates provides Ru<sup>3+</sup> ions, a chemical reaction amongst Ru<sup>3+</sup> and OH<sup>-</sup> forms Ru(OH)<sub>3</sub>, which decomposes to well-adherent RuO<sub>2</sub>. The adherent dark black RuO<sub>2</sub> thin films are formed at the temperature of deposition. At optimized substrate temperature, reaction can be,



Gujar et al. [32] have previously reported a similar reaction for RuO<sub>2</sub> films.

The gravimetric weight difference method was used to measure the film thickness of RuO<sub>2</sub> films. A sensitive microbalance was used to measure the masses of RuO<sub>2</sub> films. The variation of film

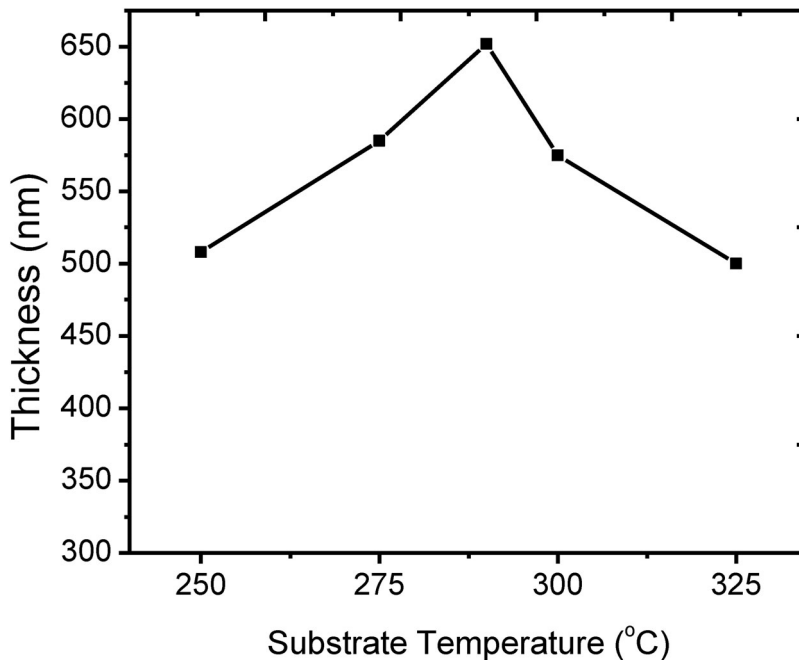


**Figure 1.** Variation of film thickness with substrate temperature for spray deposited RuO<sub>2</sub> thin films. This figure shows the variation of film thickness with substrate temperature for spray deposited ruthenium oxide thin films.

thickness for spray-deposited  $\text{RuO}_2$  films with substrate temperature is shown in Figure 1. For the  $\text{RuO}_2$  film spray deposited at  $290^\circ\text{C}$  substrate temperature, a thickness of 652 nanometers is discovered, which is comparatively higher. The film thickness is seen to increase as the substrate temperature rises, from 508 nanometers ( $250^\circ\text{C}$ ) to 652 nanometers ( $290^\circ\text{C}$ ), attaining a maximum at 652 nanometers ( $290^\circ\text{C}$ ), after which it declines to 500 nanometers ( $325^\circ\text{C}$ ). The temperature is initially insufficient to dissolve the sprayed  $\text{Ru}^{3+}$  and  $\text{O}^{2-}$  ion droplets from the solution and reduce its thickness at low substrate temperatures, such as  $250^\circ\text{C}$ . Decomposition takes place at the best rate at a specified substrate temperature of  $290^\circ\text{C}$ , producing a  $\text{RuO}_2$  terminal thickness. The re-evaporation of the material after  $\text{RuO}_2$  film deposition, thermal convection of the sprayed droplet during the spray-deposition, or both together may be responsible for the reduction in  $\text{RuO}_2$  film thickness with rising substrate temperature over  $290^\circ\text{C}$ . A similar behavior was reported for FTO thin films [35].

### 3.2. X-ray diffraction

Figure 2 displays the XRD patterns within  $2\theta$  angles  $10$ – $85^\circ$  of  $\text{RuO}_2$  films. XRD patterns exhibit a wide hump and distinct diffraction peaks, indicating the polycrystalline nature of  $\text{RuO}_2$  films. The broad hump observed in the XRD pattern (Figure 2) is due to the amorphous glass substrates used for spray deposition of  $\text{RuO}_2$  films.  $\text{RuO}_2$  films are polycrystalline regardless of substrate temperature.  $\text{RuO}_2$  film deposited at  $250^\circ\text{C}$  showed no evidence of crystallization. As the temperature of the substrate rises after  $275^\circ\text{C}$ , diffraction lines begin to develop. An increment of the substrate's

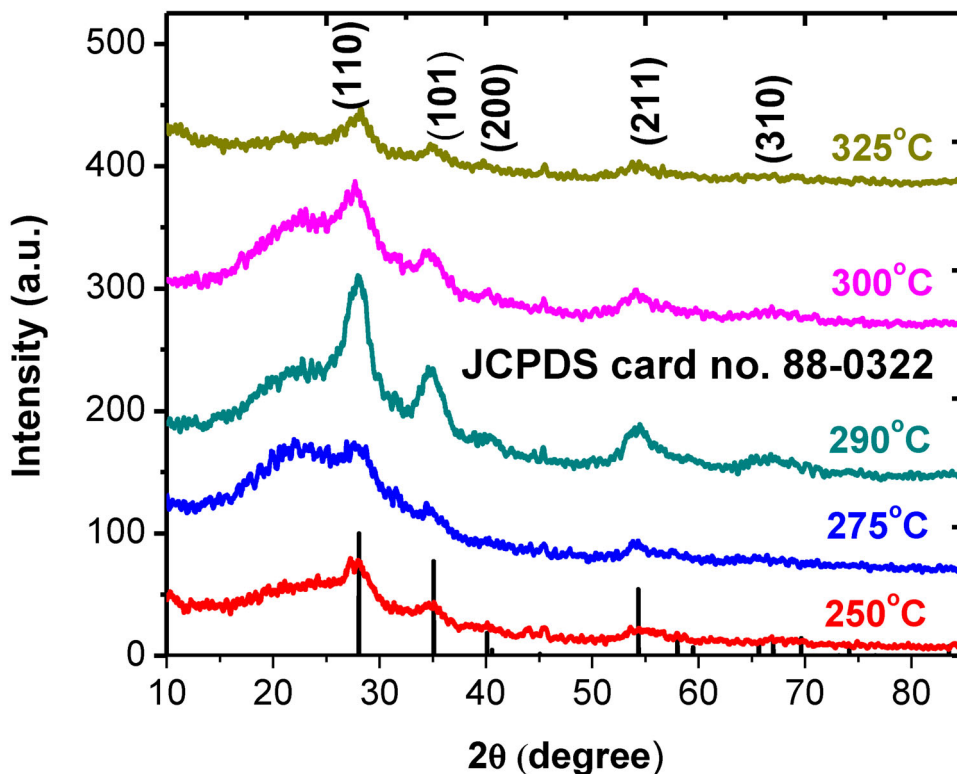


**Figure 2.** The XRD patterns of  $\text{RuO}_2$  thin films spray deposited at various substrate temperatures. This figure shows the X-ray diffraction patterns of ruthenium oxide thin films spray deposited at various substrate temperatures of 250 degree centigrade, 275 degree centigrade, 290 degree centigrade, 300 degree centigrade and 325 degree centigrade, respectively. For comparison, the database reference JCPDS (88-0322) has been added.

temperature to 290°C increases sharpness of the diffraction peaks, which corresponds to an ordering of the structure with increasing substrate temperature used for spray deposition of RuO<sub>2</sub> films. However, from the XRD pattern, we can see that the line width of the diffraction peaks becomes increasingly narrow with rise in substrate temperature after 250–290°C. Above 290°C, the diffraction peak broadens. This behavior is attributed to nanocrystallinity and local disorder. The main characteristic diffraction peaks for all samples of RuO<sub>2</sub> films are around 28.06°, 35.09°, 40.10°, 54.33° and 65.65° corresponding to (1 1 0), (1 0 1), (2 0 0), (2 1 1) and (3 1 0) plane of rutile RuO<sub>2</sub> (JCPDS card no. 88-0322) [36]. For comparison, the database reference JCPDS (88-0322) has been added.

The obtained interplanar spacing match standard values, indicating that the spray-deposited films are made of RuO<sub>2</sub> with a space group P42 rutile tetragonal crystal structure. The presence of sharp rutile RuO<sub>2</sub> peaks and the lack of any peaks connected to other RuO<sub>2</sub> phases point to the exceptional purity and crystallinity of the thin RuO<sub>2</sub> films that were spray-deposited. From Figure 2, the XRD shows the major contribution of the (1 1 0) plane. The (1 1 0) is the most thermodynamically stable plane for rutile-structured materials [37]. Therefore, rutile RuO<sub>2</sub> thin films are predicted to grow preferentially along the (1 1 0) plane under optimal conditions. These results are reliable with those obtained by Foelske et al. [38] for hydrous RuO<sub>2</sub> and by Neupane et al. [39] for thermal evaporated ruthenium dioxide nanostructures.

Using following conventional relation and knowing interplanar spacing ( $d$ ) and the Miller indices (hkl); the lattice parameters ‘ $a$ ’ and ‘ $c$ ’ were found,

$$\frac{1}{d^2} = \left( \frac{h^2 + k^2}{a^2} \right) + \frac{l^2}{c^2} \quad (4)$$

Lattice parameters for tetragonal RuO<sub>2</sub> are  $a = b = 4.5413 \text{ \AA}$  and  $c = 3.1979 \text{ \AA}$ , they correspond well with the standard lattice parameters  $a = b = 4.4930 \text{ \AA}$  and  $c = 3.1063 \text{ \AA}$  (JCPDS Card No. 88-0322).

Scherer’s formula was used to calculate the size of the crystallite [40,41],

$$D = \frac{k\lambda}{\beta \cdot \cos\theta} \quad (5)$$

where  $k$  varies from 0.89 to 1.39, but is assumed to be one in the present case,  $\lambda = 1.5406 \text{ \AA}$ ,  $\beta$  is the FWHM and  $\theta$  is the Bragg angle. The crystallite size was determined for (1 1 0) plane. It increases from 14 nm to 16 nm with changing substrate temperature from 250°C to 290°C. For increasing temperature of substrates from 290°C to 325°C, the crystallite size decreases from 16 to 13 nanometers. Since the deposited atoms condense and remain fixed to the area to form small nuclei and clusters, rather than integrating to the nearby crystallites and increasing their size, the crystallite size is small at lower substrate temperatures (250°C). As atoms’ surfaces become more mobile and cluster formation increases at a higher substrate temperature of 290°C, a larger crystallite size is seen. At a substrate temperature of 290°C, it is shown that the crystallite size grows and reaches a maximum of 16 nm. By raising the substrate temperature, a decrease in lattice strain was seen. In fact, the strain in the films is tensile in the beginning of RuO<sub>2</sub> film formation and goes toward compression and lattice strain during the terminal stages of RuO<sub>2</sub> film formation. For the film formed at the substrate temperature of 290°C, the lowest values of dislocation density and stacking probability are obtained. The dislocation density of as-prepared RuO<sub>2</sub> films decreased as the substrate temperature increased. The change in crystallite size with substrate temperature explained this behavior. These values of crystallite size are comparable to 23 nm reported by Devdas et al. for hydrous RuO<sub>2</sub> [42]. The structural data for RuO<sub>2</sub> films is shown in Table 1.

The pore-specific volumes for RuO<sub>2</sub> electrodes spray deposited at various substrate temperatures obtained from the BET surface area measurements are listed in Table 2. The fact that pore-specific volume is larger for substrate temperature of 290°C compared to other samples suggest the RuO<sub>2</sub>

**Table 1.** Structural data for RuO<sub>2</sub> thin films prepared by spray pyrolysis at various substrate temperatures.

Ts (°C)	2θ (°)	d (Å) (Cal.)	d (Å) (Std.)	hkl	a (Å)	c (Å)	D (nm)
250	27.52	3.238	3.177	110	4.542	3.174	14
	34.44	2.602	2.555	101			
	40	2.252	2.247	200			
	53.82	1.702	1.687	211			
275	27.31	3.263	3.177	110	4.614	3.228	15
	33.86	2.645	2.555	101			
	53.82	1.702	1.687	211			
290	27.82	3.204	3.177	110	4.517	3.168	16
	34.55	2.594	2.555	101			
	40	2.252	2.247	200			
	54.2	1.691	1.687	211			
	66.43	1.406	1.421	310			
300	27.54	3.236	3.177	110	4.54	3.222	15
	34.09	2.628	2.555	101			
	40	2.252	2.247	200			
	53.68	1.706	1.687	211			
	66.39	1.407	1.421	310			
325	28.12	3.17	3.177	110	4.494	3.198	13
	34.39	2.605	2.555	101			
	40	2.252	2.247	200			
	53.82	1.702	1.687	211			

Ts, substrate temperature; 2θ, Bragg's angle; d, interplanar spacing; hkl, miller indices; a,c lattice constants; D, crystallite size.

electrode spray deposited at substrate temperatures of 290°C possesses much higher micropores than other samples; therefore it contains more inner active surface sites.

### 3.3. FESEM and EDAX

FESEM images of spray-deposited RuO<sub>2</sub> electrodes are illustrated in [Figure 3](#) at a magnification of ×200k. RuO<sub>2</sub> thin films are homogeneous, compact and compliant in nature. Morphology characteristics of RuO<sub>2</sub> films muscularly depend on substrate temperature used for deposition. RuO<sub>2</sub> thin films spray deposited at 250°C substrate temperature show small spherical grains covering the entire substrate surface. As the substrate temperature reaches 275°C, the average grain size upsurges and RuO<sub>2</sub> films begin to become porous. At 290°C substrate temperature, the controlled agglomeration of smaller particles results in the formation of bigger particles in the porous RuO<sub>2</sub> layer. This high order, homogeneous morphology is important for the use of RuO<sub>2</sub> films in electrochemical supercapacitor applications. A similar porous morphology has been reported by Jana et al. [43] for NiO thin films. With more rise in temperature of substrates above 290°C, the porous nature of the RuO<sub>2</sub> thin films decreases ([Table 2](#)) and cannot be distinguished with small spherical grains. At 325°C substrate temperature, the size of small spherical grains decreases.

EDAX analysis was performed to clearly understand the elemental structure of RuO<sub>2</sub> films. [Figure 4](#) depicts a typical EDAX spectrum of a RuO<sub>2</sub> thin film spray deposited at 290°C substrate temperature. The compositional data of RuO<sub>2</sub> films produced by spray pyrolysis at different substrate temperatures is given in [Table 3](#). From EDAX studies, formation of RuO<sub>2</sub> is confirmed.

**Table 2.** BET surface area results of RuO<sub>2</sub> thin films prepared by spray pyrolysis at various substrate temperatures.

Substrate Temp. (°C)	True surface area (10 <sup>3</sup> cm <sup>2</sup> )	Pore-specific volume (10 <sup>3</sup> cm <sup>3</sup> g <sup>-1</sup> )
250	0.983	7.628
275	1.072	8.784
290	1.191	9.790
300	1.057	8.634
325	0.954	7.508

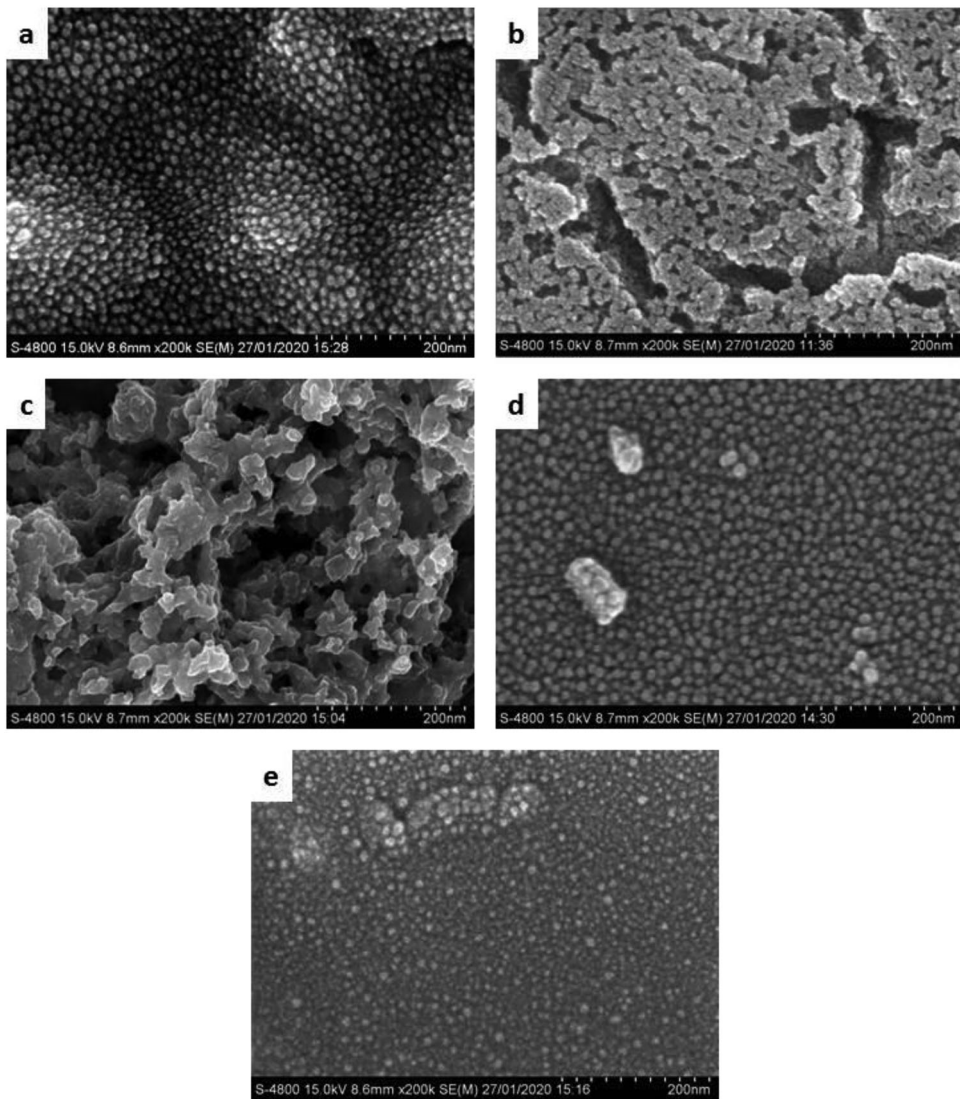


**Figure 3.** FESEM images of morphology evolution for  $\text{RuO}_2$  thin films spray deposited at various substrate temperatures (a) 250° C, (b) 275°C, (c) 290°C, (d) 300°C and (e) 325°C, respectively. This figure shows the FESEM images of morphology evolution for ruthenium oxide thin films spray deposited at various substrate temperatures of 250 degree centigrade, 275 degree centigrade, 290 degree centigrade, 300 degree centigrade and 325 degree centigrade, respectively.

EDAX spectrum revealed stoichiometric formation of  $\text{RuO}_2$ . With change in temperature of substrates, the ratio of Ru/O in the film is changed.

**Table 3.** Compositional analysis of  $\text{RuO}_2$  thin films prepared by spray pyrolysis at various substrate temperatures.

Substrate Temp. (°C)	Atomic percentage in $\text{RuO}_2$ thin films	
	Ru	O
250	35.98	64.02
275	34.56	65.44
290	31.28	68.72
300	30.67	69.33
325	30.29	69.71

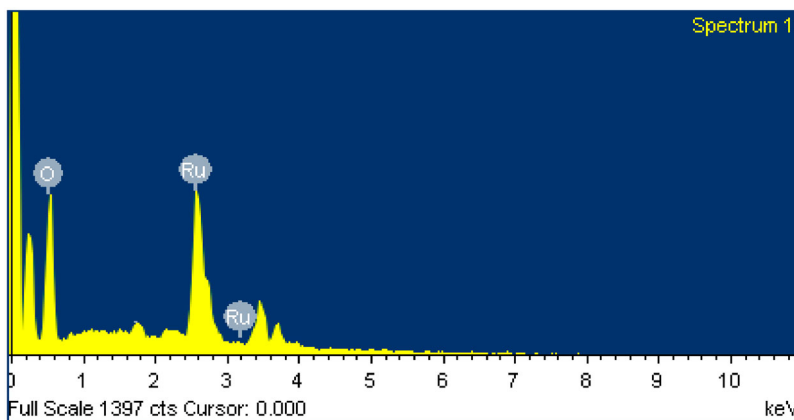


**Figure 4.** EDAX spectrum of as-deposited RuO<sub>2</sub> thin film (substrate temperature 290°C). This figure shows the EDAX spectrum of as-deposited ruthenium oxide thin film at substrate temperature 290 degree centigrade.

### 3.4. Optical

By capturing UV-Visible optical absorption spectra in the 350–1050 nm wavelength range, optical properties of RuO<sub>2</sub> films were examined. RuO<sub>2</sub> films have extraordinary absorbance in the visible region, indicating their potential as absorbent materials. The bandgap of spray-deposited RuO<sub>2</sub> thin films was found from absorption data and by applying the well-known Tauc's relation [44,45]. To determine bandgap of RuO<sub>2</sub> films,  $(\alpha h\nu)^2$  versus  $h\nu$  were plotted as shown in Figure 5(a). Straight lines in the high-energy domain signify direct optical transitions. The bandgap of 2.05 eV was obtained for RuO<sub>2</sub> film spray-deposited at 250°C. For 290°C substrate temperature, the optical bandgap decreases to 1.90 eV and further increases to 2.13 eV for 325°C substrate temperature. The bandgap for spray-deposited RuO<sub>2</sub> films varies with substrate temperature as seen in Figure 5(b) and Table 4. These values are close to the threshold bandgap of 1.8 eV obtained for RuO<sub>2</sub> single crystal [46] and comparable to 1.87 eV reported by Farid El-Tantawy et al. [47] for ruthenium dioxide, and 2.2 eV reported by Patake and Lokhande [34] for chemically synthesized nano-porous RuO<sub>2</sub>. These values of bandgap make RuO<sub>2</sub> films useful as materials for optoelectronic devices.

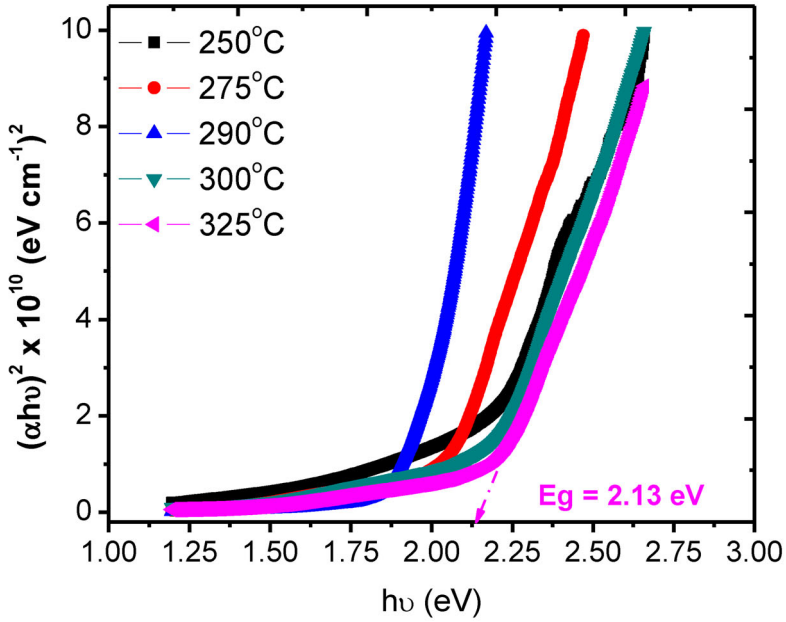
### 3.5. Electrical

The electrical properties of RuO<sub>2</sub> films were studied in 300–500 K by DC two-point probe technique. Table 4 depicts electrical parameters of RuO<sub>2</sub> films. Figure 6 shows the plot of  $\log(\rho)$  versus  $1000/T$  for RuO<sub>2</sub> films. The film resistivity of RuO<sub>2</sub> decreased with growing operating temperature indicating semiconducting behavior, though metallic behavior was reported for RuO<sub>2</sub> films [48]. RuO<sub>2</sub> thin film show different electrical resistivity values. A room temperature electrical resistivity of  $1.05 \times 10^4 \Omega\text{-cm}$  was acquired for RuO<sub>2</sub> film spray deposited at 250°C substrate temperature,

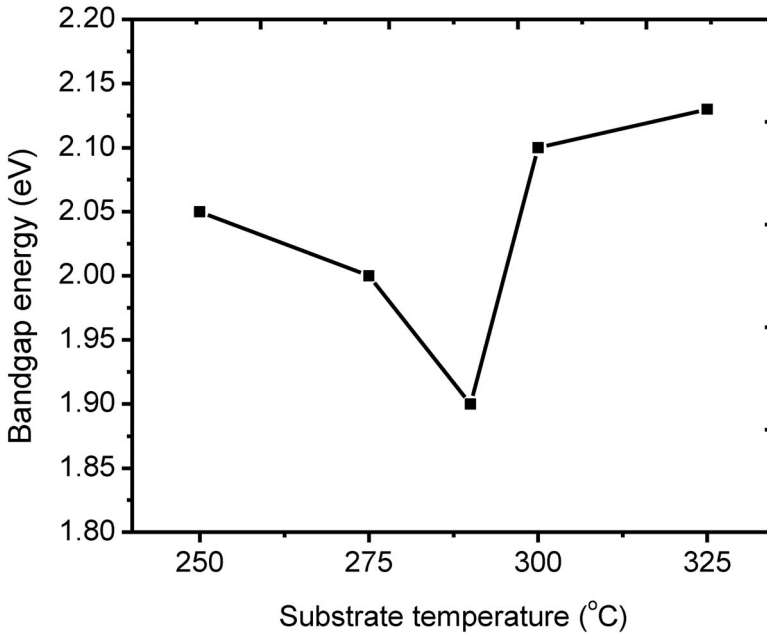
**Table 4.** Optical and electrical properties of RuO<sub>2</sub> thin films prepared by spray pyrolysis at various substrate temperatures.

Substrate Temp. (°C)	Band gap (eV)	Electrical resistivity ( $\Omega\text{-cm}$ )		Activation energy (eV)	
		300 K ( $\times 10^4$ )	500 K ( $\times 10^2$ )	LT	HT
250	2.05	1.05	11.3	0.055	0.041
275	2	0.68	7.67	0.052	0.041
290	1.9	0.57	6.35	0.054	0.044
300	2.1	0.91	9.27	0.057	0.045
325	2.13	1.23	13.06	0.055	0.04

LT, low temperature; HT, high temperature.



(a)



(b)

**Figure 5.** (a) Typical variation of  $(\alpha h\nu)^2$  as a function of  $h\nu$  used for determination optical bandgap and (b) variation of bandgap energy with substrate temperature for RuO<sub>2</sub> thin films. (a) Shows the typical variation of  $(\alpha h\nu)^2$  as a function of  $h\nu$  used for determination optical bandgap for ruthenium oxide thin films prepared by spray pyrolysis at various substrate temperatures of 250 degree centigrade, 275 degree centigrade, 290 degree centigrade, 300 degree centigrade and 325 degree centigrade respectively. (b) Variation of bandgap energy with substrate temperature for ruthenium oxide thin films.

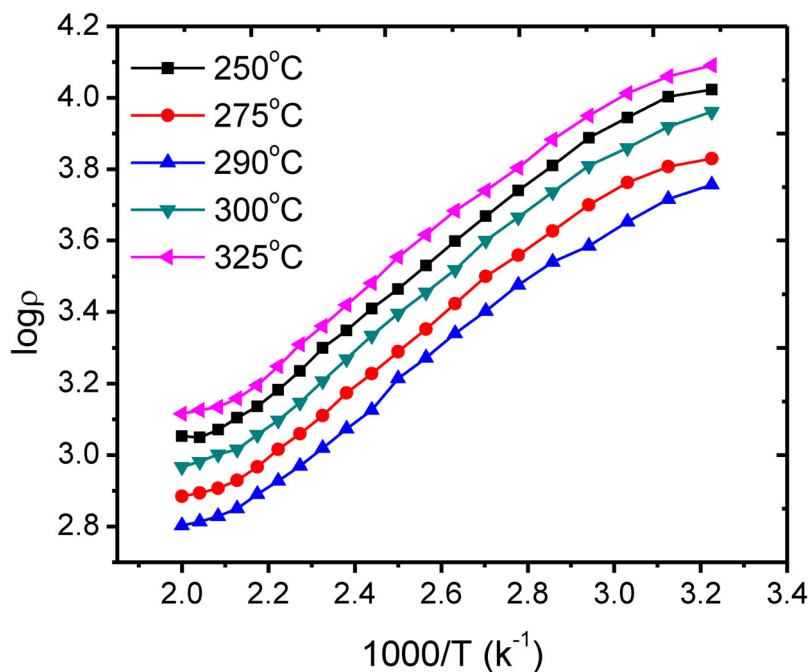


**Figure 6.** Plot of  $\log(\rho)$  versus  $1000/T$  for  $\text{RuO}_2$  thin films spray deposited at various substrate temperatures. This figure shows variation of  $\log \rho$  with inverse of absolute temperature ( $1000/T$ ) for ruthenium oxide thin films prepared by spray pyrolysis at various substrate temperatures of 250 degree centigrade, 275 degree centigrade, 290 degree centigrade, 300 degree centigrade and 325 degree centigrade, respectively.

which decreased with increasing substrate temperature to a minimum ( $0.57 \times 10^4 \Omega\text{-cm}$ ) for  $\text{RuO}_2$  film deposited at 290°C substrate temperature. A high room temperature electrical resistivity ( $1.23 \times 10^4 \Omega\text{-cm}$ ) is witnessed for  $\text{RuO}_2$  film spray deposited at 325°C substrate temperature. These values of electrical resistivity are comparable with values reported by Patake and Lokhande [34] for chemically synthesized nano-porous  $\text{RuO}_2$  films.

$\text{RuO}_2$  films exhibit Arrhenius behavior. Activation energies of  $\text{RuO}_2$  films were calculated using the relation [40]. The trap level's location below the conduction band is indicated by the activation energy. Activation energies are 0.052–0.057 eV and 0.041–0.045 eV in the low-temperature and high-temperature regions, correspondingly. These values are smaller than the 2.1–2.4 eV obtained by Ribera et al. [49].

### 3.6. Electrochemical

#### 3.6.1. CV

Using CV over a broad potential range from 0.0 to 1.0 V (Ag/AgCl in 0.5 M  $\text{H}_2\text{SO}_4$ ), the electrochemical presentation of  $\text{RuO}_2$  films was examined. As seen from Figure 7(a–e), due to high electrical resistivity of  $\text{RuO}_2$ , which significantly contributes to the overall equivalent series resistance, the CV curves are consistently slanted at lower scan rates, there are no noticeable redox peaks, and CVs are deviated from the ideal rectangle. Figure 8(a) shows CV plots at  $10 \text{ mVs}^{-1}$  of  $\text{RuO}_2$  films in 0.5 M  $\text{H}_2\text{SO}_4$  electrolyte. Using a relation previously provided elsewhere [50], CV curves were used to measure the specific capacitance of  $\text{RuO}_2$  films and results are tabulated as Table 5. Figure 8(b) depicts the change of specific capacitance ( $C_{\text{sp}}$ ) with scan rate for  $\text{RuO}_2$  films. From graph, the specific capacitance,  $C_{\text{sp}}$  decreased from  $687 \text{ Fg}^{-1}$  to  $514 \text{ Fg}^{-1}$ , as the scan rate was increased from  $5 \text{ mVs}^{-1}$  to  $100 \text{ mVs}^{-1}$  for  $\text{RuO}_2$  film deposited at 290°C substrate

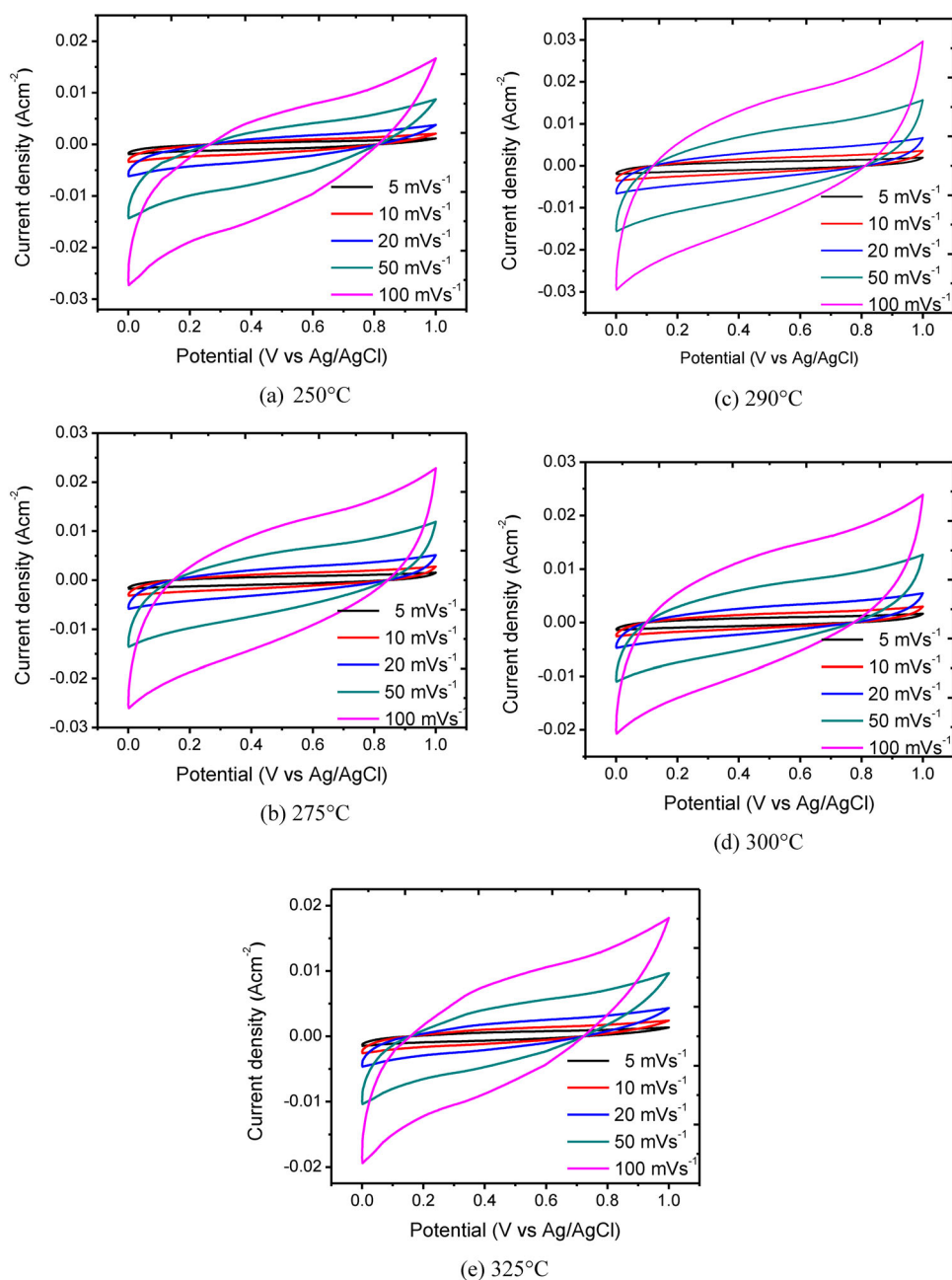
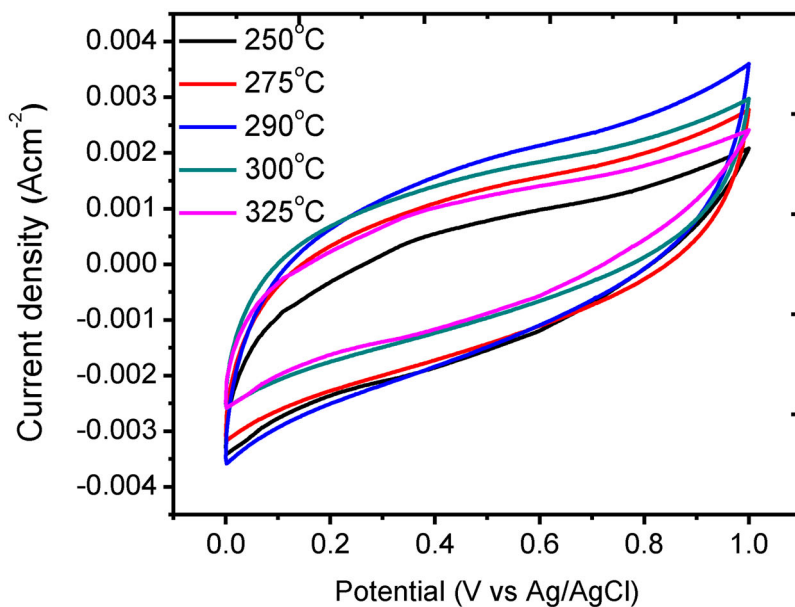
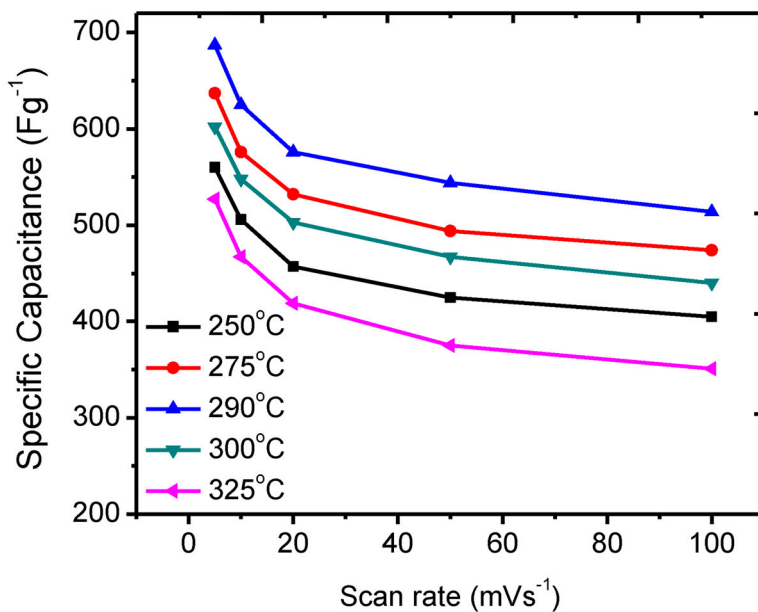


**Figure 7.** CV Plots at scan rates of 5–100  $\text{mVs}^{-1}$  for  $\text{RuO}_2$  thin films prepared by spray pyrolysis at various substrate temperatures (a) 250°C, (b) 275°C, (c) 290°C, (d) 300°C and (e) 325°C, respectively. This figure shows CV Plots at scan rates of 5–100  $\text{mVs}^{-1}$  for ruthenium oxide thin films prepared by spray pyrolysis at various substrate temperatures of 250 degree centigrade, 275 degree centigrade, 290 degree centigrade, 300 degree centigrade and 325 degree centigrade, respectively.

temperature. This illustrates the voltammetric current dependence on scan rate. A decrease in the capacitance with scan rate of the  $\text{RuO}_2$  electrode can be due to increase in ionic resistance [51]. The decreasing trend of capacitance with increasing scan rate indicates that parts of  $\text{RuO}_2$  film electrode surface are unreachable at higher scan rates. Therefore, the specific capacitance at lower scan rates is considered the closest towards full utilization of  $\text{RuO}_2$  film electrode material



(a)



(b)

**Figure 8.** (a) CV plots at scan rate of  $10 \text{ mVs}^{-1}$  and (b) variation of specific capacitance with scan rate for  $\text{RuO}_2$  thin films prepared by spray pyrolysis at various substrate temperatures. (a) Shows CV plots at scan rate of 10 millivolt per second for ruthenium oxide thin films prepared by spray pyrolysis at various substrate temperatures of 250 degree centigrade, 275 degree centigrade, 290 degree centigrade, 300 degree centigrade and 325 degree centigrade, respectively. (b) shows variation of specific capacitance with scan rate for ruthenium oxide thin films prepared by spray pyrolysis at various substrate temperatures.

**Table 5.** Specific capacitance at different scan rates from CV for RuO<sub>2</sub> thin films prepared by spray pyrolysis at various substrate temperatures.

Substrate temperature (°C) → scan rate (mVs <sup>-1</sup> ) ↓	250	275	290	300	325
	Specific capacitance from CV (Fg <sup>-1</sup> )				
5	560	637	687	602	527
10	506	576	625	548	467
20	457	532	576	503	419
50	425	494	544	467	375
100	405	474	514	440	351

[52]. A high specific capacitance of 687 Fg<sup>-1</sup> obtained in present study is higher than 209 Fg<sup>-1</sup> at 5 mVs<sup>-1</sup> for ruthenium oxide nanoparticles [53] and is comparable to 650 Fg<sup>-1</sup> reported by Patake et al. [54] for electrodeposited RuO<sub>2</sub> films and 606 Fg<sup>-1</sup> by Raja et al. [55] for RuO<sub>2</sub> particles.

### 3.6.2. GCD

GCD helps to characterize the electrochemical stability of RuO<sub>2</sub> thin film electrodes for a huge number of GCD cycles over wider potential ranges under constant current density [56]. Figure 9 presents GCD curves of RuO<sub>2</sub> thin film electrodes in 0.5 M H<sub>2</sub>SO<sub>4</sub> electrolyte, in 0.0–0.85 V potential window. The quasisymmetric shape of the GCD specifies the capacitive behavior of RuO<sub>2</sub> film electrode. Three zones can be seen on charge–discharge curves: a quick potential decrease followed by a slow potential decline. The capacitive property of RuO<sub>2</sub> film electrode is characterized by the abrupt potential drop and subsequent potential decline caused by the internal resistance of RuO<sub>2</sub> film electrode. The second zone represents the double-layer capacitance and exhibits linear behavior in the time dependency of the potential. The third zone is the potential's slope dependency, which results from redox reactions in the pseudocapacitance at the interface between the RuO<sub>2</sub> electrode and the 0.5 M H<sub>2</sub>SO<sub>4</sub> electrolyte.

The GCD curves with a current density of 1 Ag<sup>-1</sup> are depicted in Figure 10(a). With rise in substrate temperature used for the spray deposition of RuO<sub>2</sub> film, the discharge time upsurges up to 290°C substrate temperature and reduces thereafter. Following relationships [56] were used to compute specific capacity (C<sub>s</sub>), specific energy (SE) and specific power (SP) and the results are given in Table 6,

$$C_s = \frac{I \times \Delta t}{m \times \Delta V} \quad (6)$$

$$SE = \frac{1/4CV^2}{3.6} \quad (7)$$

$$SP = \frac{3600 \times SE}{t} \quad (8)$$

Where symbols used have their usual meaning. A plot of specific capacitance against current density for RuO<sub>2</sub> electrodes prepared by spray pyrolysis can be seen in Figure 10(b). The calculated specific capacitance for RuO<sub>2</sub> electrode deposited at 290°C substrate temperature was 741 Fg<sup>-1</sup> at

**Table 6.** Specific capacitances from GCD for RuO<sub>2</sub> thin films prepared by spray pyrolysis at various substrate temperatures.

Substrate temperature (°C) → Current density (Ag <sup>-1</sup> ) ↓	250	275	290	300	325
	Specific capacitance from GCD (Fg <sup>-1</sup> )				
0.5	605	686	741	650	569
1	546	622	675	591	504
2	493	574	622	543	452
4	459	533	586	503	405

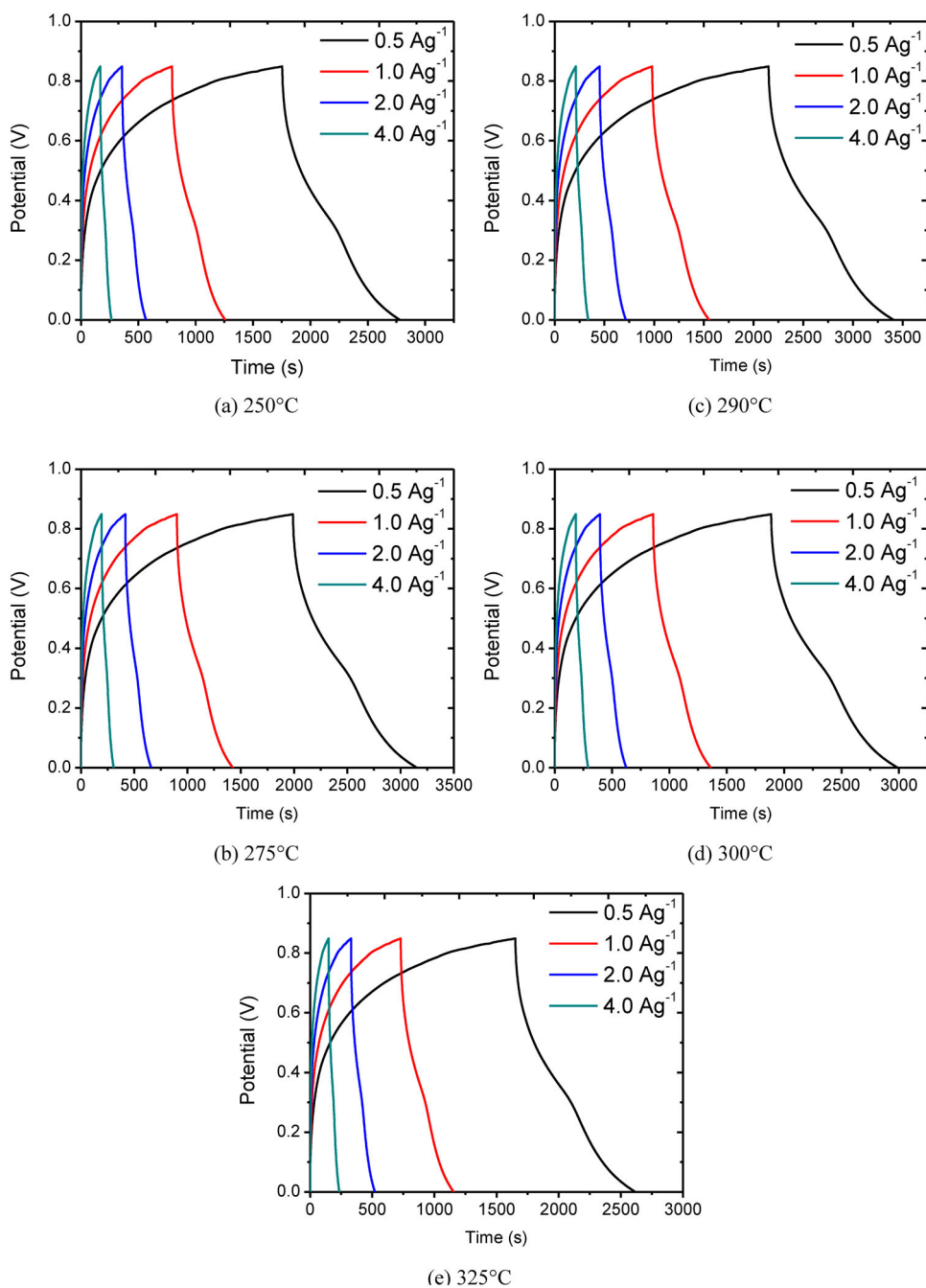
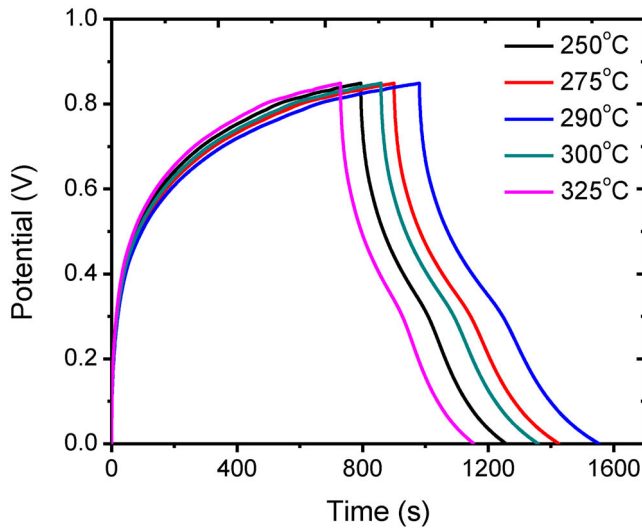
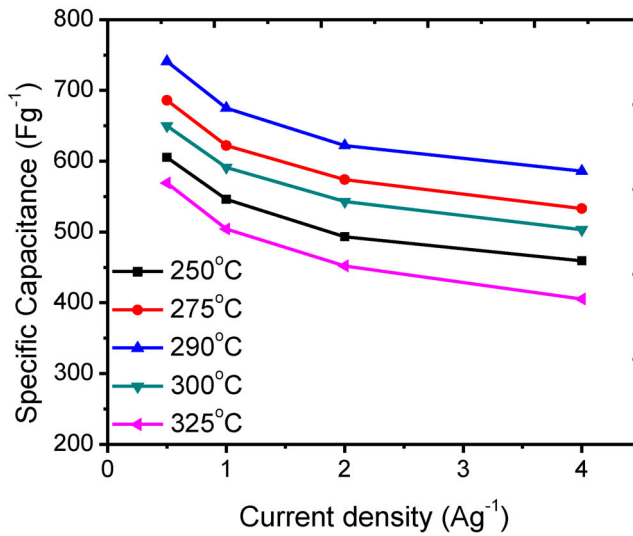


**Figure 9.** GCD curves at different current densities for RuO<sub>2</sub> thin films prepared by spray pyrolysis at substrate temperatures of (a) 250°C, (b) 275°C, (c) 290°C, (d) 300°C and (e) 325°C, respectively. This figure shows GCD curves at different current densities for ruthenium oxide thin films prepared by spray pyrolysis at various substrate temperatures of 250 degree centigrade, 275 degree centigrade, 290 degree centigrade, 300 degree centigrade and 325 degree centigrade, respectively.

0.5 Ag<sup>-1</sup>, which lessened to only 586 Fg<sup>-1</sup> at 4 Ag<sup>-1</sup> current density. This specific capacitance is more than 200 Fg<sup>-1</sup> at 1 Ag<sup>-1</sup> current density, which was recently reported for RuO<sub>2</sub> nanoplatelets by Sarkar et al. [57] and 276 Fg<sup>-1</sup> were obtained at 13.33 Ag<sup>-1</sup> for RuO<sub>2</sub> by Mondal and



(a)



(b)

**Figure 10.** (a) GCD curves at current density of  $1 \text{ Ag}^{-1}$  and (b) plot of specific capacitance versus current density for  $\text{RuO}_2$  electrodes prepared by spray pyrolysis at various substrate temperatures. (a) GCD curves at current density of one ampere per gram for ruthenium oxide thin films prepared by spray pyrolysis at various substrate temperatures of 250 degree centigrade, 275 degree centigrade, 290 degree centigrade, 300 degree centigrade and 325 degree centigrade, respectively. (b) Shows the plot of specific capacitance versus current density for ruthenium oxide electrodes prepared by spray pyrolysis at various substrate temperatures of 250 degree centigrade, 275 degree centigrade, 290 degree centigrade, 300 degree centigrade and 325 degree centigrade, respectively.

Munichandraiah [58]. Table 7 summarizes the recent research works that were carried out in the literature for  $\text{RuO}_2$ -based systems, including different electrolytes employed.

The specific energy plotted against the specific power (Ragone plot) of the  $\text{RuO}_2$  film deposited at  $290^\circ\text{C}$  substrate temperature is shown in Figure 11(a). The SP and SE are  $1694 \text{ Wkg}^{-1}$  and

**Table 7.** The capacitive performance comparison of RuO<sub>2</sub> films in this work with various RuO<sub>2</sub> reported in some literatures.

Order	Material	Electrolyte	Measurement protocol	Max. capacitance	Reference
1	RuO <sub>2</sub> NNs/Ta/Cu	diluted H <sub>2</sub> SO <sub>4</sub>	GCD@50 mAcm <sup>-2</sup>	580 Fg <sup>-1</sup>	[26]
2	RuO <sub>2</sub> /Lipon/RuO <sub>2</sub> /Pt	Lipon	GCD@100 μAcm <sup>-2</sup>	38 mFcm <sup>-2</sup>	[27]
3	RuO <sub>2</sub>	0.5 M H <sub>2</sub> SO <sub>4</sub>	CV@5 mVs <sup>-1</sup>	551 Fg <sup>-1</sup>	[32]
4	RuO <sub>2</sub>	0.5 M H <sub>2</sub> SO <sub>4</sub>	CV@20 mVs <sup>-1</sup>	50 Fg <sup>-1</sup>	[34]
5	RuO <sub>2</sub>	0.5 M H <sub>2</sub> SO <sub>4</sub>	CV@5 mVs <sup>-1</sup>	209 Fg <sup>-1</sup>	[53]
6	RuO <sub>2</sub>	0.5 M H <sub>2</sub> SO <sub>4</sub>	CV@20 mVs <sup>-1</sup>	650 Fg <sup>-1</sup>	[54]
7	RuO <sub>2</sub>	1 M H <sub>2</sub> SO <sub>4</sub>	GCD@0.1A g <sup>-1</sup>	111 Fg <sup>-1</sup>	[55]
8	RuO <sub>2</sub>	1 M KOH	GCD@0.8A g <sup>-1</sup>	200 Fg <sup>-1</sup>	[57]
9	RuO <sub>2</sub>	0.5 M H <sub>2</sub> SO <sub>4</sub>	GCD@13.33A g <sup>-1</sup>	276 Fg <sup>-1</sup>	[58]
10	RuO <sub>2</sub>	0.5 M H <sub>2</sub> SO <sub>4</sub>	CV@2 mVs <sup>-1</sup>	73 Fg <sup>-1</sup>	[59]
11	This work	0.5 M H <sub>2</sub> SO <sub>4</sub>	CV@5 mVs <sup>-1</sup>	687 Fg <sup>-1</sup>	
	This work	0.5 M H <sub>2</sub> SO <sub>4</sub>	GCD@0.5 Ag <sup>-1</sup>	741 Fg <sup>-1</sup>	

58.80 Whkg<sup>-1</sup>, respectively, at 4 Ag<sup>-1</sup>; comparable to SE values of 3.57 Wh kg<sup>-1</sup> and SP values of 151 Wkg<sup>-1</sup> reported by Patil et al. [59] for hydrous RuO<sub>2</sub>. The SE and SP values are in Ragone plots designed specifically for supercapacitor applications [60].

The long-term cycling performance at 1 Ag<sup>-1</sup> current density is shown in Figure 11(b) for 3000 cycles of RuO<sub>2</sub> film spray deposited at 290°C substrate temperature. The RuO<sub>2</sub> film electrode's specific capacitance keeps 87.66% of its first value, which shows good cycle stability. The inset of Figure 11(b) shows the charging–discharging curve of the RuO<sub>2</sub> film in the last five cycles, it displays a nearly identical symmetrical shape, showing that charge–discharge processes do not significantly alter the structure of the RuO<sub>2</sub> film electrode.

### 3.6.3. EIS

EIS studies were performed in 0.5 M H<sub>2</sub>SO<sub>4</sub> to extend our understanding of the electrochemical behavior of RuO<sub>2</sub> thin film electrodes. Typical Nyquist plots of RuO<sub>2</sub> electrodes are shown in Figure 12. RuO<sub>2</sub> electrodes exhibit good capacitive behavior, with a semicircle in the high-frequency zone and linear section in the low-frequency region that is more inclined to the imaginary axis (showing a vertical line) [61]. An expanded picture of the RuO<sub>2</sub> electrodes' semicircles may be seen in the inset of Figure 12. Table 8 shows the data obtained from Nyquist plots for RuO<sub>2</sub> films. Good values of 0.40Ω solution resistance and 17.10 Ωcm<sup>2</sup> charge transfer resistance were perceived for RuO<sub>2</sub> electrodes prepared at 290°C substrate temperature.

## 4. Conclusions

A simple chemical spray pyrolysis was utilized to deposit RuO<sub>2</sub> thin film electrodes for supercapacitor application. The rutile phase of RuO<sub>2</sub> with a porous structure with small spherical grains was formed. Optical studies presented a direct bandgap between 1.90 and 2.13 eV for spray-deposited RuO<sub>2</sub> thin film electrodes. A maximum specific capacitance of 687 Fg<sup>-1</sup> at 5 mV s<sup>-1</sup> in a 0.5 M H<sub>2</sub>SO<sub>4</sub> electrolyte was observed. Furthermore, RuO<sub>2</sub> device transported a great specific capacitance of 741 Fg<sup>-1</sup> at 0.5 Ag<sup>-1</sup> current density with an extraordinary power density (1694 Wkg<sup>-1</sup>), energy density (58.80 Whkg<sup>-1</sup>) and good cycle-life (87.66% after 3000 cycles). This study deduces that use

**Table 8.** Nyquist data for RuO<sub>2</sub> thin films prepared by spray pyrolysis at various substrate temperatures.

Substrate temperature (°C)	Rs (Ω)	Rct (Ωcm <sup>2</sup> )
250	0.7	35.64
275	0.55	24.75
290	0.4	17.1
300	0.6	28.15
325	0.85	41.27

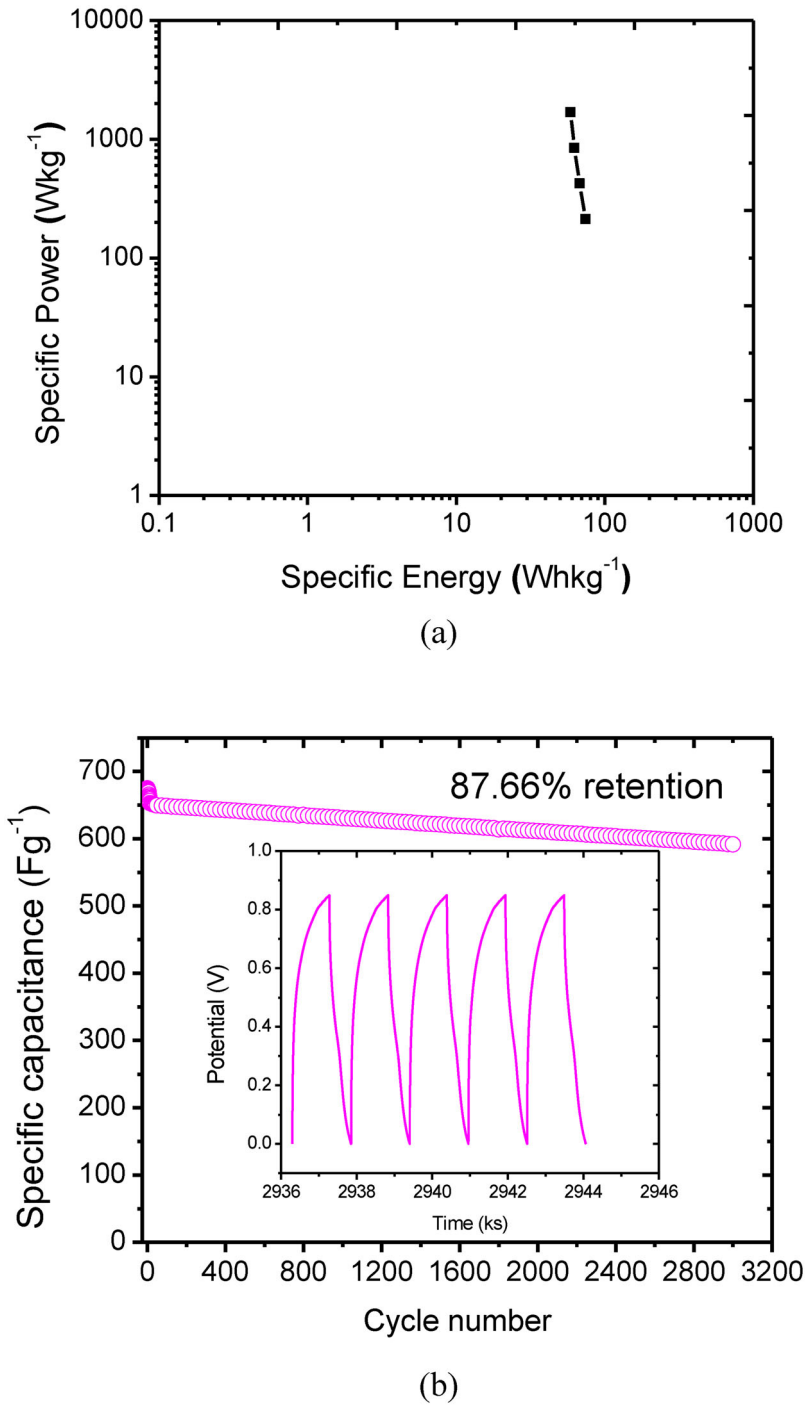


**Figure 11.** (a) Ragone plot of  $\text{RuO}_2$  thin film electrode prepared at substrate temperature of  $290^\circ\text{C}$  and (b) Long-term cycling performance of the  $\text{RuO}_2$  thin films spray deposited at substrate temperature of  $290^\circ\text{C}$  and at the current density of  $1 \text{ Ag}^{-1}$ . The inset shows the charge–discharge curves of the last five cycles of the  $\text{RuO}_2$  thin films. (a) Shows the Ragone plot of ruthenium oxide thin film electrode prepared at substrate temperature of 290 degree centigrade. (b) Shows the long-term cycling performance of the ruthenium oxide thin films spray deposited at substrate temperature of 290 degree centigrade and at the current density of one ampere per gram. The inset shows the charge-discharge curves of the last five cycles of the ruthenium oxide thin films.

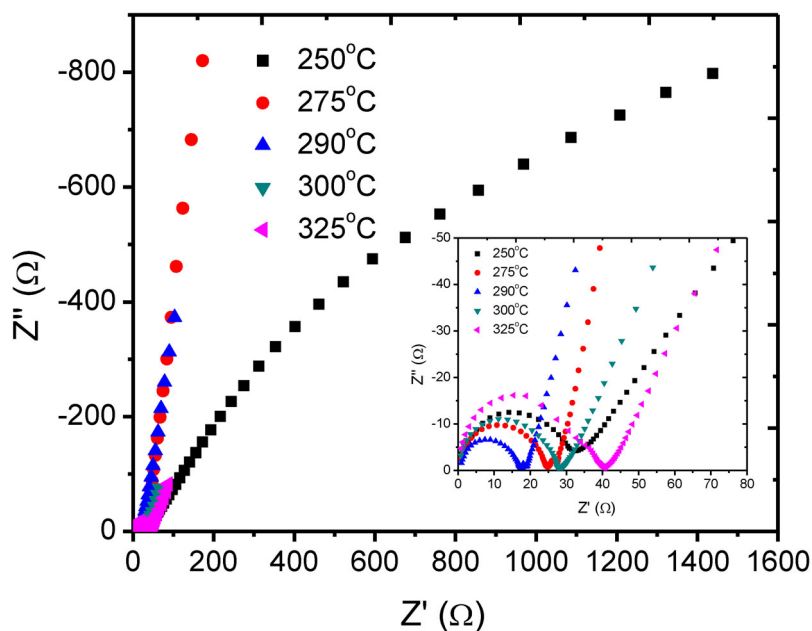


**Figure 12.** Nyquist plot for RuO<sub>2</sub> thin film electrodes prepared by spray pyrolysis at various substrate temperatures. This figure shows the Nyquist plot for ruthenium oxide thin films prepared by spray pyrolysis at various substrate temperatures of 250 degree centigrade, 275 degree centigrade, 290 degree centigrade, 300 degree centigrade and 325 degree centigrade respectively. The inset shows the enlarged view of Nyquist plots.

aqueous/organic solvent mixture improves physico-chemical and morphological characteristics of RuO<sub>2</sub> films.

### Disclosure statement

No potential conflict of interest was reported by the author(s).

### ORCID

Abhijit A. Yadav  <http://orcid.org/0000-0002-3486-4099>

### References

- [1] Güneri E, Aker D, Henry J, et al. Cu<sub>2</sub>O thin films prepared by chemical bath deposition: an improved method. *Phase Transit.* 2022;95(10):679–690.
- [2] Patil NM, Nilange SG, Jundale VA, et al. Structural, optical and electrical properties of spray-deposited Fe-doped nanocrystalline ZnS<sub>0.2</sub>Se<sub>0.8</sub> thin films. *Phase Transit.* 2021;94(6-8):493–510.
- [3] Poonam KS, Arora A, Tripathi SK. Review of supercapacitors: materials and devices. *J Energy Storage.* 2019;21:801–825.
- [4] Jundale VA, Patil DA, Yadav AA. Preparation and characterization of NiFe<sub>2</sub>O<sub>4</sub> thin films for supercapacitor applications. *Phase Transit.* 2022;95(11):786–802.
- [5] Thomas ABG, Gupta RK. Nanostructured materials for supercapacitors. Springer International Publishing; 2022.
- [6] Chikkegowda CR, Yadav AA. Precursor solution concentration-dependent electrochemical supercapacitive behavior of spray-deposited RuO<sub>2</sub> films using aqueous/organic solvent mixtures. *J Appl Electrochem.* 2022. DOI:10.1007/s10800-022-01806-7
- [7] Zheng Y, Yang H, Lin Y, et al. Preparation of hollow carbon rods by using ZnO as template for high-performance supercapacitor. *J Mater Sci Mater Electron.* 2021;32:8491–8502.

- [8] Chandrashekar R, Yadav AA. Spray-deposited cobalt-doped RuO<sub>2</sub> electrodes for high-performance supercapacitors. *Electrochim Acta*. 2023;437:141521.
- [9] Liu Y, Jiang SP, Shao Z. Intercalation pseudocapacitance in electrochemical energy storage: recent advances in fundamental understanding and materials development. *Mater Today Adv*. 2020;7:100072.
- [10] Chodankar NR, Pham HD, Nanjundan AK, et al. True meaning of pseudocapacitors and their performance metrics: asymmetric versus hybrid supercapacitors. *Small*. 2020;16(37):2002806.
- [11] Chen X, Paul R, Dai L. Carbon-based supercapacitors for efficient energy storage. *Natl Sci Rev*. 2017;4:453–489.
- [12] Pandolfo AG, Hollenkamp AF. Carbon properties and their role in supercapacitors. *J Power Sources*. 2006;157:11–27.
- [13] Zhi M, Xiang C, Li J, et al. Nanostructured carbon-metal oxide composite electrodes for supercapacitors: a review. *Nanoscale*. 2013;5:72–88.
- [14] Stoller MD, Magnuson CW, Zhu YW, et al. Interfacial capacitance of single layer graphene. *Energ Environ Sci*. 2011;4:4685–4689.
- [15] <https://www.mpoweruk.com/performance.htm>
- [16] Lokhande CD, Dubal DP, Joo O-S. Metal oxide thin film based supercapacitors. *Curr Appl Phys*. 2011;11:255–270.
- [17] Zhao Y, Chen Y, Liu Q, et al. Construction of cobaltous oxide/nickel–iron oxide electrodes with great cycle stability and high energy density for advanced asymmetry supercapacitor. *J Mater Sci Mater Electron*. 2019;30:21219–21228.
- [18] Fang T-Y, Zeng Y-Z, Liu Y-C, et al. High-performance asymmetric supercapacitors fabricated by amorphous MnO<sub>2</sub> on 3D-Ni foam as positive electrodes in a mixed electrolyte. *J Mater Sci Mater Electron*. 2020;31:7672–7682.
- [19] Kour S, Tanwar S, Sharma AL. A review on challenges to remedies of MnO<sub>2</sub> based transition-metal oxide, hydroxide, and layered double hydroxide composites for supercapacitor applications. *Mater Today Commun*. 2022;32:104033.
- [20] Yadav AA. Physical and electrochemical properties of spray deposited Co<sub>3</sub>O<sub>4</sub> thin films. *Phase Transit*. 2021;94(10):691–704.
- [21] Naiknaware AG, Chavan JU, Kaldete SH, et al. Studies on spray deposited Ni doped Mn<sub>3</sub>O<sub>4</sub> electrodes for supercapacitor applications. *J Alloys Comp*. 2019;774:787–794.
- [22] Yadav AA, Chavan UJ. Electrochemical supercapacitive performance of spray-deposited NiO electrodes. *J Electron Mater*. 2018;47(7):3770–3778.
- [23] Yadav AA, Chavan UJ. Electrochemical supercapacitive performance of spray deposited Co<sub>3</sub>O<sub>4</sub> thin film nanostructures. *Electrochim Acta*. 2017;232:370–376.
- [24] Zhang Y, Li L, Su H, et al. Binary metal oxide: advanced energy storage materials in supercapacitors. *J Mater Chem A*. 2015;3:43–59.
- [25] Iro ZS, Subramani C, Dash SS. A brief review on electrode materials for supercapacitor. *Int J Electrochem Sci*. 2016;11:10628–10643.
- [26] Cho S, Kim J, Han J, et al. Self-assembled RuO<sub>2</sub> nanoneedles on Ta/Cu foil for a robust and high-performance supercapacitor electrode. *Surf. Interfaces (Providence)*. 2022;31:102069.
- [27] Lim JH, Choi DJ, Kim H-K, et al. Thin film supercapacitors using a sputtered RuO<sub>2</sub> electrode. *J Electrochem Soc*. 2001;148:A275.
- [28] Karatum O, Yildiz E, Kaleli HN, et al. RuO<sub>2</sub> supercapacitor enabled flexible, safe, and efficient optoelectronic neural interface. *Adv Funct Mater*. 2022;32:2109365.
- [29] Gao Y, Zheng D, Li Q, et al. 3D Co<sub>3</sub>O<sub>4</sub>-RuO<sub>2</sub> hollow spheres with abundant interfaces as advanced trifunctional electrocatalyst for water-splitting and flexible Zn-Air battery. *Adv Funct Mater*. 2022;32:2203206.
- [30] Wang W, Wang K, Hao W, et al. Preparation of Ti-based Yb-doped SnO<sub>2</sub>-RuO<sub>2</sub> electrode and electrochemical oxidation treatment of coking wastewater. *J Rare Earths*. 2022;40:763–771.
- [31] Arvizu MA, González FJ, Romero-Galarza A, et al. Symmetric supercapacitors of PANI coated RuO<sub>2</sub>/TiO<sub>2</sub> macroporous structures prepared by electrostatic spray deposition. *J Electrochem Soc*. 2022;169:020564.
- [32] Gujar TP, Shinde VR, Lokhande CD, et al. Spray deposited amorphous RuO<sub>2</sub> for an effective use in electrochemical supercapacitor. *Electrochem Commun*. 2007;9:504–510.
- [33] Fugare BY, Lokhande BJ. Study on structural, morphological, electrochemical and corrosion properties of mesoporous RuO<sub>2</sub> thin films prepared by ultrasonic spray pyrolysis for supercapacitor electrode application. *Mater Sci Semicond Process*. 2017;71:121–127.
- [34] Patake VD, Lokhande CD. Chemical synthesis of nano-porous ruthenium oxide (RuO<sub>2</sub>) thin films for supercapacitor application. *Appl Surf Sci*. 2008;254:2820–2824.
- [35] Yadav AA, Masumdar EU, Moholkar AV, et al. Electrical, structural and optical properties of SnO<sub>2</sub>:F thin films: effect of the substrate temperature. *J Alloys Compd*. 2009;488:350–355.
- [36] JCPDS 88-0322.
- [37] Lister TE, Tolmachev YV, Chu Y, et al. Cathodic activation of RuO<sub>2</sub> single crystal surfaces for hydrogen-evolution reaction. *J Electroanal Chem*. 2003;554:71–76.

- [38] Foelske A, Barbieri O, Hahn M, et al. An X-ray photoelectron spectroscopy study of hydrous ruthenium oxide powders with various water contents for supercapacitors. *Electrochem Solid-State Lett.* 2006;9:A268–A272.
- [39] Neupane S, Kaganas G, Valenzuela R, et al. Synthesis and characterization of ruthenium dioxide nanostructures. *J Mater Sci.* 2011;46:4803–4811.
- [40] Yadav AA, Jadhav SN, Chougule DM, et al. Spray deposited Hausmannite  $Mn_3O_4$  thin films using aqueous/organic solvent mixture for supercapacitor applications. *Electrochim Acta.* 2016;206:134–142.
- [41] Henry J, Daniel T, Balasubramanian V, et al. Synthesis and characterisation of  $Cu_2Se$  thin films doped with divalent cation ( $Cd^{2+}$ ) by the chemical bath deposition method. *Phase Transit.* 2021;94:567–576.
- [42] Devadas A, Baranton S, Coutanceau C. Green synthesis and modification of  $RuO_2$  materials for the oxygen evolution reaction, front. *Energy Res.* 2020;8:571704.
- [43] Jana S, Mondal G, Mitra BC, et al. Facile synthesis of nickel oxide thin films from PVP encapsulated nickel sulfide thin films: an efficient material for electrochemical sensing of glucose, hydrogen peroxide and photo-degradation of dye. *New J Chem.* 2017;41:14985–14994.
- [44] Shetty C, Shastrimath VVD, Bairy R. Tuning the structural, morphological and optical properties of Sr-doped BFO thin films. *Phase Transit.* 2022;95(3):202–211.
- [45] Ganesh Kumar K, Balaji Bhargav P, Gnana Prakash D, et al. Investigations on SILAR coated CZTS thin films for solar cells applications. *Phase Transit.* 2021;94(6-8):556–566.
- [46] Belkind A, Orban Z, Vossen JL, et al. Optical properties of  $RuO_2$  films deposited by reactive sputtering. *Thin Solid Films.* 1992;207:242–247.
- [47] El-Tantawy F, Al-Ghamdi AA, Al-Ghamdi AA, et al. Optical properties of nanostructured ruthenium dioxide thin films via sol-gel approach. *J Mater Sci Mater Electron.* 2017;28:52–59.
- [48] Baumann PK, Doppelt P, Fröhlich K, et al. Platinum, ruthenium and ruthenium dioxide electrodes deposited by metal organic chemical vapor deposition for oxide applications. *Integr Ferroelectr.* 2002;44:135–142.
- [49] Coloma Ribera R, van de Kruijs RWE, Yakshin AE, et al. Determination of oxygen diffusion kinetics during thin film ruthenium oxidation. *J Appl Phys.* 2015;118:055303.
- [50] Yadav AA, Chavan UJ. Electrochemical supercapacitive performance of spray deposited  $NiSnO_3$  thin films. *Thin Solid Films.* 2017;634:33–39.
- [51] Convey BE, Pell WG. Proceedings of the eighth international seminar on double layer capacitors and similar energy storage devices, Deerfield Beach, FL, December 1998.
- [52] Gujar TP, Shinde VR, Lokhande CD, et al. Electrosynthesis of  $Bi_2O_3$  thin films and their use in electrochemical supercapacitors. *J Power Sources.* 2006;161:1479–1485.
- [53] Nisha B, Vidyalakshmi Y, Razack SA. Enhanced formation of ruthenium oxide nanoparticles through green synthesis for highly efficient supercapacitor applications. *Adv Powder Technol.* 2020;31:1001–1006.
- [54] Patake VD, Lokhande CD, Joo OS. Electrodeposited ruthenium oxide thin films for supercapacitor: effect of surface treatments. *Appl Surf Sci.* 2009;255:4192–4196.
- [55] Raja A, Son N, Swaminathan M, et al. Electrochemical behavior of heteroatom doped on reduced graphene oxide with  $RuO_2$  for HER, OER, and supercapacitor applications. *J Taiwan Inst Chem Eng.* 2022;138:104471.
- [56] Majumdar D, Maiyalagan T, Jiang Z. Recent progress in ruthenium oxide-based composites for supercapacitor applications. *ChemElectroChem.* 2019;6:4343–4372.
- [57] Sarkar S, Mukherjee D, Harini R, et al. Ionic liquid-assisted synthesis of tri-functional ruthenium oxide nanoplatelets for electrochemical energy applications. *J Mater Sci.* 2022;57:7680–7693.
- [58] Mondal SK, Munichandraiah N. Anodic deposition of porous  $RuO_2$  on stainless steel for supercapacitor studies at high current densities. *J Power Sources.* 2008;175:657–663.
- [59] Patil UM, Kulkarni SB, Jamadade VS, et al. Chemically synthesized hydrous  $RuO_2$  thin films for supercapacitor application. *J Alloys Comp.* 2011;509:1677–1682.
- [60] Burke A. Ultracapacitors: why, how, and where is the technology. *J Power Sources.* 2000;91:37–50.
- [61] Amir FZ, Pham VH, Dickerson JH. Facile synthesis of ultra-small ruthenium oxide nanoparticles anchored on reduced graphene oxide nanosheets for high performance supercapacitors. *RSC Adv.* 2015;5:67638–67645.